Nuclear Instruments and Methods in Physics Research A 1065 (2024) 169471

Contents lists available at ScienceDirect

Nuclear Inst. and Methods in Physics Research, A

journal homepage: www.elsevier.com/locate/nima

Full Length Article

Simulations of a cryogenic, buffer-gas filled Paul trap for low-emittance ion bunches

S. Lechner [a,b,c,*], S. Sels [a], I. Belosevic [d], F. Buchinger [c], P. Fischer [e], C. Kanitz [f], V. Lagaki [a,e], F.M. Maier [a,e], P. Plattner [a,g], L. Schweikhard [e], M. Vilen [a], S. Malbrunot-Ettenauer [a,d,h]

[a] Experimental Physics Department, CERN, CH-1211 Geneva 23, Switzerland
[b] Technische Universität Wien, AT-1040, Wien, Austria
[c] McGill University, Montréal, Québec, H3A 2T8, Canada
[d] TRIUMF, Vancouver, BC V6T 2A3, Canada
[e] Institut für Physik, Universität Greifswald, 17487 Greifswald, Germany
[f] Department für Physik, Friedrich-Alexander-Universität Erlangen-Nürnberg, 91058 Erlangen, Germany
[g] Universität Innsbruck, AT-6020, Innsbruck, Austria
[h] Department of Physics, University of Toronto, Toronto M5S 1A7, Canada

ARTICLE INFO

Keywords:
Paul trap
MIRACLS
Collinear laser spectroscopy
MR-toF
Exotic radionuclides
Buffer-gas cooling

ABSTRACT

Many experiments with pulsed ion beams benefit from or even require ion bunches with both small temporal width as well as small energy spread. To achieve optimal ion-beam preparation, a buffer-gas filled cryogenic Paul trap is being developed in the context of the Multi Ion Reflection Apparatus for Collinear Laser Spectroscopy (MIRACLS). There, ion bunches of short-lived radionuclides are trapped in a Multi-Reflection Time-of-Flight (MR-ToF) device. Thus, the ions can be repeatedly probed by a laser beam compared to only once in conventional, single-passage collinear laser spectroscopy. To fulfill MIRACLS' opposing requirements of a small temporal ion-bunch width and small energy spread, a buffer-gas filled cryogenic Paul trap is envisioned. Ion-optical simulations confirm the advantages of cryogenic temperatures and the linear scaling of the beam emittance as a function of the buffer-gas temperature. Beyond MIRACLS, high-quality ion beams from a cryogenic Paul trap will be beneficial for other precision experiments at radioactive ion beam facilities.

1. Introduction

The well established technique of fluorescence-based collinear laser spectroscopy (CLS) enables high-precision studies of electromagnetic properties in short-lived radionuclides [1–3]. However, for the exploration of the most exotic nuclides far away from stability, more sensitive experimental methods have to be envisioned. The yields of such nuclei at radioactive ion beam (RIB) facilities can be as low as a few ions per second delivered to experiments. This renders conventional, fluorescence-based CLS experiments – with typical detection limits of 10^3 to 10^4 ions per second – unfeasible [4]. The Multi Ion Reflection Apparatus for Collinear Laser Spectroscopy (MIRACLS) [5–10] at ISOLDE/CERN is a new approach to overcome these limitations by performing CLS measurements in a Multi-Reflection Time of Flight (MR-ToF) device [11–25]. In such a trap, ion bunches bounce back and forth between two electrostatic mirrors. This allows repeated probing of the ion ensemble by the spectroscopy laser. Hence, rare isotopes are utilized more efficiently compared to conventional, single-passage CLS which greatly enhances the sensitivity. Combined with ion-beam energies of around 30 keV, unprecedented in an MR-ToF apparatus, the high spectral resolution of conventional CLS can be preserved.

The combination of CLS and MR-ToF techniques in MIRACLS constitutes stringent requirements on the emittance of the probed ion bunches. A low energy spread ($\Delta E \lesssim 1$ eV) to minimize the CLS Doppler broadening is as essential as a temporally narrow ion-bunch profile ($\Delta t \lesssim 500$ ns) for MR-ToF operation. The latter is important to efficiently inject the ion bunch into the finite length of the MR-ToF device and to benefit from a narrow ion-bunch structure resulting in an improved signal-to-background ratio in CLS measurements [10]. Moreover, the transverse emittance should be as small as possible to obtain optimal geometrical overlap of the ion and laser beam while the ion trajectories are as parallel as possible to the laser-beam axis. Therefore, high quality

* Corresponding author at: Experimental Physics Department, CERN, CH-1211 Geneva 23, Switzerland.
E-mail address: simon.lechner@cern.ch (S. Lechner).

https://doi.org/10.1016/j.nima.2024.169471
Received 22 November 2023; Received in revised form 27 April 2024; Accepted 21 May 2024
Available online 23 May 2024

ion-bunch preparation is required. For this purpose, a cryogenic, buffer-gas filled Paul trap to cool ions below 40 K has been envisioned for a next-generation application of MIRACLS.

As already reported in the 1990s [26], the emittance of ion bunches in these traps, also called cooler-bunchers, scales linearly with the buffer-gas temperature. Thus, a cryogenic trap will be able to provide ion bunches of very low emittance. Such a device will best address the demands of CLS and MR-ToF operation with maximal benefit for CLS sensitivity even though the very first science goals at MIRACLS can already be reached using a room-temperature Paul trap [10]. Specialized cooler-bunchers have explored the advantages of cryogenic environments cooled by liquid nitrogen [27,28], however, most devices for beam cooling and bunching at RIB facilities operate at room temperature due to their reduced technical complexity.

The interest in developing a cryogenic cooler-buncher also reflects a general push towards next-generation precision experiments at RIB facilities. Thus, in addition to MIRACLS, other ion-trap or laser-spectroscopy applications will profit from the high-quality ion bunches provided by such a cryogenic Paul trap. Among others, these include laser spectroscopy and future precision studies with radioactive molecules [29,30] or the antiProton Unstable Matter Annihilation (PUMA) project for the combination of anti-matter with radioactive nuclides [31].

In this work, ion-optical simulations are carried out to identify a suitable design of MIRACLS' cryogenic Paul trap. The key design requirements for this trap are listed as follows:

- An acceptance that allows to efficiently capture high-emittance beams delivered by ISOLDE, i.e. up to $\sim 6\,\pi$ mm mrad (rms).
- Cryogenic cooling of the ion trap to liquid-helium temperatures to obtain very cold ion samples and thus low-emittance beams of short-lived radionuclides.
- Minimization of a re-heating effect during ion extraction, i.e. the elimination of ion collisions with helium buffer gas along the re-acceleration path upon ejection from the Paul trap.[1]
- A compact trap design reflecting existing space constraints at ISOLDE while facilitating easy maintenance.

After a brief review of the relevant Paul trap principles in Section 2, the general trap design is introduced in Section 3. The discussion of the simulation results is organized along the topics of injection into the Paul trap in Section 4.1, transfer between two pressure regions in Section 4.2, ion-bunch extraction in Section 4.3 and space-charge effects in Section 4.3.3.

2. Paul trap principles

In order to confine charged particles in a linear Paul trap, a time-dependent radio-frequency field in radial direction is combined with a static axial potential [36]. This creates an effective potential minimum in all 3 dimensions and enables stable ion storage. The approximate hyperbolic electric potential in radial direction is established by positioning cylindrical rod electrodes in a quadrupole configuration, and can be written as

$$\Phi = \frac{\Phi(t)}{2r_0^2}(x^2 - y^2), \tag{1}$$

with r_0 being the edge-to-edge half-distance between opposing electrodes. $\Phi(t)$ is a time-dependent potential difference between adjacent rods. The form of the time-dependent potential can be either given as $\Phi(t) = V\sin(\omega t)$ for a sinusoidal radio-frequency (RF) driver or $\Phi(t) = VS_\delta$ for a square-wave field. Here, V is the amplitude of the RF field and ω its angular frequency. For a square-wave driven instruments, a duty cycle of 50% is commonly used, alternating between $\pm V$. Operation in this mode has first been introduced in Ref. [37] and corresponding devices are now commonly known as digital ion traps (DIT) [38,39]. Their square-wave driven RF field [40] offers some advantages over conventional sinusoidal RF fields. When the square wave is generated by fast high-voltage switches, broadband operation across a wide range of RF frequencies can be achieved without the need for a tuned circuit, i.e. the RF frequency and amplitude can be readily adopted to the respective ion mass and charge. Furthermore, the pseudo potential is deeper in such a DIT compared to a sinusoidal trap for the same RF amplitude and frequency [39,40].

From Eq. (1) the ions' equation of motion can be derived, which has the form of the Meissner equations for square-wave fields [40]. The dimensionless stability parameter is defined as [40,41]

$$q = \frac{4ZeV}{m\omega^2 r_0^2}, \tag{2}$$

where Z denotes the ions' charge state, e represents the elementary charge and m is the ion mass.

Solving the equation of motion reveals that the radial ion motion inside a Paul trap is governed by a slow harmonic motion (macro motion), which is perturbed by a fast micro motion [36,40]. The stability of the ion motion depends on the parameter q. This implies that only certain combinations of RF frequency and amplitude lead to a stable ion confinement in radial direction. Up to $q \approx 0.712$ ions can be trapped in a square-wave driven Paul trap [40] (or $q \approx 0.908$ in sinusoidally-driven traps).

2.1. Buffer-gas cooling

In addition to trapping and storing ions, Paul traps are also used to cool ions. In the realm of rare isotope science, a commonly used and versatile technique to prepare high-quality beams is buffer-gas cooling [26,42]. A buffer gas at pressures of 10^{-2} to 10^{-4} mbar is typically inserted into the trap. Trapped ions undergo collisions with the buffer gas, which thermalizes the ion ensemble to the buffer-gas temperature. This simultaneously results in the concentration of the ion bunch at the axial potential minimum of the trap. By switching the endcap potential of the Paul trap to a lower voltage, a cooled ion bunch with low emittance can be extracted and delivered to subsequent experiments.

In many cases helium (He) is the gas of choice given its high ionization energy limiting the risk of ion loss due to charge exchange, but also other noble gases are used, especially for higher ion masses. Advantages of buffer-gas cooling are the fast thermalization in the order of milliseconds and the applicability to all elements from He to the heaviest species (He^+ ions require H_2 buffer gas). These two aspects explain the attractiveness of this cooling method for RIB facilities.

2.2. Ion-beam emittance

The ion-beam quality is typically characterized in terms of its emittance. In the context of bunched ion beams, it is important to differentiate between the longitudinal emittance ξ_{long}, which corresponds to the product of the ion bunch's temporal width and its energy spread $\xi_{\text{long}} \approx \pi \cdot \Delta E \cdot \Delta t$ at the time-focus point, and the transverse emittance ξ_{trans}. The latter is related to the spatial (Δx) and angular ($\Delta\Theta$) distribution of a beam in the direction perpendicular to the ion-beam propagation. At the spatial focus point, $\xi_{\text{trans}} \approx \pi \cdot \Delta x \cdot \Delta\Theta$ holds. Assuming a harmonic trap potential, the longitudinal emittance for ions extracted from a buffer-gas filled, linear Paul trap can be derived as [26,27]

$$\xi_{95\%,\text{long}} \approx 2\pi \ln(20)\frac{k_B T}{\omega_z}, \tag{3}$$

[1] This effect is mentioned in Ref. [28,32–34] but, to our knowledge, has not been studied in detail. Note that it is not related to RF heating in buffer-gas filled Paul traps [35,36].

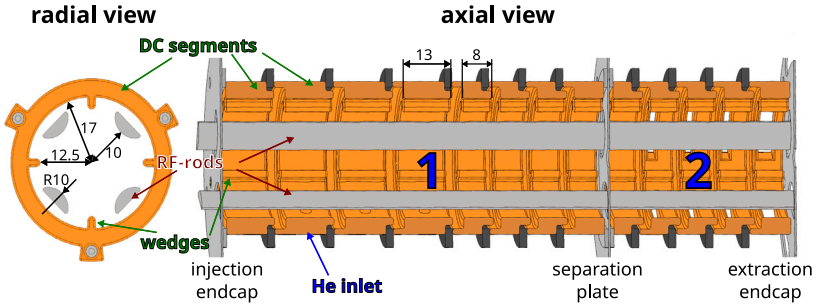

Fig. 1. Radial and axial cross section of the trap geometry. All dimensions are given in mm. The radius R of the quadrupole rods is 10 mm, same as r_0 from Eq. (1). The beam enters from the left through the injection endcap, is cooled and accumulated in the high pressure region **1**. Afterwards it is sent through the separation plate to the low pressure region **2**. The entrance and exit hole at the two endcaps both have a radius of 2.5 mm. The trap consists of 13 DC-segments, the first four with a length of 13 mm and the rest with 8 mm, separated by 2 mm, which adds up to a total trap length of 15 cm. Insulators (black) separate the DC electrodes.

where ω_z is the longitudinal oscillation frequency in the Paul trap. The transverse emittance follows

$$\xi_{95\%,\mathrm{trans}} \approx 2\pi \ln(20) \frac{k_B T}{\omega_m \sqrt{2mE}}. \quad (4)$$

Here, ω_m is the radial macro-motion frequency and E the ion-beam energy after re-acceleration. Note that Eq. (3) and (4) refer to 95% of the ions from a given ensemble. At LEBIT, a very good agreement between experimental and theoretical emittance has been found [27]. The linear dependence of the ion-beam emittance on the buffer-gas temperature motivates the development of a cryogenic cooler-buncher for advanced ion-beam preparation. It is, however, important to stress that these formulas are only valid if there is no ion-cloud re-heating present during the extraction and re-acceleration process. Moreover, a deep axial well potential counteracts the radial confinement [43] and thus may also increase the transverse emittance.

3. Trap design and concept of operation

Since the first application of a linear Paul trap for accumulation, cooling and bunching of radioactive ion beams around 20 years ago [43], a lot of effort has been invested into the design of these radio-frequency-quadrupole (RFQ) cooler and bunchers. The MIRACLS Paul trap has taken inspiration from several existing devices [27,28,40,44] and adopts some of their features to attain a simple and compact design.

A configuration with four truncated RFQ rods for radial confinement and separate DC ring electrodes with inwardly directed "wedges" perpendicular to the rods for axial confinement is chosen as shown in Fig. 1. In this design, the application of the RF field is simplified compared to the case in which it has to be individually coupled to segmented rod electrodes which provide both DC and RF fields. A drawback of our approach is, however, the reduced field strength of the DC elements due to shielding by the RFQ rods. To overcome the need for very high voltages, wedges are introduced to increase the effective DC field inside the trap. The circular DC electrodes are held at fixed positions by insulating spacers in between. The electrodes are shaped in a way to remove the spacers from the ions' line of sight. This prevents charge-up of the insulators, which might otherwise negatively impact the trap's performance.

Moreover, the trap is separated into two pressure regions. In the first one, the ions are stopped efficiently by a high buffer-gas pressure, while the pressure in the second region is significantly lower to minimize the re-heating effect during re-acceleration as explained above. A separator plate (thickness = 0.5 mm, hole diameter = 6 mm) is placed between the two regions which acts as a differential pumping segment (see Fig. 1). This approach is simpler, although likely not as effective in separating the pressure compared to the solutions in Refs. [27,28], where a third intermediate trap region is present. To obtain a significant difference in pressure in our trap configuration, helium gas is exclusively injected into the high-pressure region. The endcap of the second region is designed to be permeable (i.e. by using a 50% opaque mesh) and holes in the DC segments of this region further increase the buffer-gas outflow. Latter holes additionally allow for potential radial laser access such that laser cooling inside the Paul trap could be performed to achieve even colder beams (see Ref. [45] for more details).

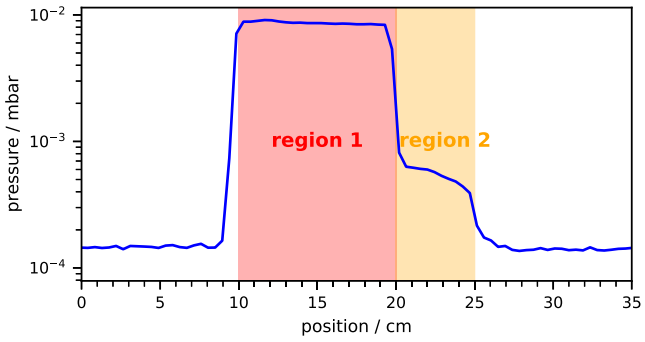

Fig. 2. Pressure along the trap axis obtained by molecular flow simulations using the software Molflow [46]. For the simulations, the trap is placed in a CF160 cross attached to a vacuum pump with a pumping power of 6551/s. Helium gas at room temperature enters the trap through an inlet located at the beginning of region 1, see Fig. 1. The pressure regions are indicated by shaded areas.

In order to estimate the achievable pressure gradient between the two trapping regions as well as to the outside of the trap, gas-flow simulations are performed. For this purpose, the software Molflow [46], which simulates the pressure distribution in the molecular flow regime [47], is employed.[2] Fig. 2 shows that the pressure outside the trap drops by around two orders of magnitude within 10 to 15 mm. Moreover, a pressure difference of around one order of magnitude can be achieved between the first and second region of the trap.

Due to the small length of 10 cm in the first region of the present trap, its capability to fully stop and capture incoming ions might not be sufficient in some cases. This is typically the case for higher masses as will be shown in Section 4.1. However, due to the simple stacking design of the DC electrodes, additional DC segments could be added easily to increase the injection efficiency for certain applications beyond MIRACLS.

[2] While the Knudsen regime might be more appropriate for the pressures utilized in buffer-gas filled Paul traps, it greatly increases the computational complexity. The molecular flow regime should give a good enough approximation, especially towards lower pressures as demonstrated in Ref. [46]. Additionally, 2-dimensional simulations in a simplified geometry have been performed with the transitional flow module of COMSOL® [48]. Their results qualitatively confirm the Molflow simulations in Fig. 2.

Following the arguments given in Section 2, a square-wave driven RF field has been chosen over conventional sinusoidal RF fields.

The Paul trap is designed to operate along the following steps. (1) The ions are decelerated by floating the Paul trap and the associated injection geometry to an electrostatic potential such that the ions enter the Paul trap at a few tens to hundred electronvolts of remaining beam energy. (2) The ions are injected into the high-pressure region 1 where they are stopped by the buffer gas and subsequently accumulated in a potential well next to the separation plate. (3) Once all injected ions are thermalized in the potential well of the high-pressure region 1, they are transferred into the low-pressure region 2. There, they are once again thermalized in another potential well located next to the extraction endcap. Finally, (4) the ions are extracted from the Paul trap and are re-accelerated. Details of the injection and the re-acceleration optics will be discussed in Sections 4.1 and 4.3, respectively.

4. Ion-optical simulations

The ion-optical simulations are carried out in SIMION [49], a widely used software tool for simulations of charged-particles optics. A user program for the implementation of the hard-sphere model [50] is used to simulate the ion-gas interactions. These SIMION simulations are additionally validated with the program IonCool [51]. IonCool is a dedicated software package for the simulation of realistic ion-buffer-gas interactions in electric fields, using the (n-4-6) potential [51], see Appendix A.2 for more details. While IonCool is deemed more accurate for low-energy collisions, SIMION simulations with the hard-sphere model are more time-efficient for our computational setup. In the present work, both models result in similar trends.

The present simulations are performed for two ion species, once for the lighter (i.e. lower m/z) $^{20}Mg^{+}$ ions, which will be an interesting first physics case for MIRACLS, as well as for heavier $^{133}Cs^{+}$ ions. For each case, the RF frequency and amplitude are adjusted to $q \approx 0.4$ (see Eq. (2)) for both respective masses and kept the same for all simulations, unless stated otherwise. For example, for $^{20}Mg^{+}$ ions an RF amplitude of 120 V at 1.2 MHz is used. Helium serves as buffer gas and is set to either room temperature (300 K) or 40 K. The latter is a rather conservative assumption, since the trap electrodes will be cooled by a 4 K, two-stage cryocooler, which will result in temperatures significantly below 40 K. The 40 K temperature in this work acts as a worst-case upper limit of the final temperature. Low pressure or high temperature lead to low gas density. Therefore, effects which are related to both, buffer-gas temperature and pressure, will be simply referred to as gas density in the following.

The results of the gas-flow simulations (see Fig. 2) are used as basis for pressure gradients in the following ion-optical simulations. For computational simplicity in SIMION and IonCool, either a constant pressure inside the trap or a linear pressure gradient between different regions is assumed, reflecting their numerical values as found in the gas-flow simulations. Outside the trap, the pressure is chosen to follow a linear pressure gradient next to the endcaps and is set to zero at longer distance from the trap.

Following the concept of operation introduced in Section 3, we simulate the performance of the Paul trap as follows. First, we perform simulations of the ion injection without considering any buffer gas (Section 4.1.1). This simulation step benchmarks different injection geometries for their efficiency in guiding ion beams of different beam quality through the hole in the injection endcap. Moreover, it investigates how well the ions could be transferred to the other side of pressure region 1 (again without the presence of a buffer gas).

Second, the injection simulation is repeated for the best-performing injection geometry of the previous step but this time also considering buffer gas (Section 4.1.2). The capture efficiency, ion losses due to different processes, as well as the averaged ion-cooling time into the potential well of pressure region 1 are studied at various buffer-gas pressures and temperatures.

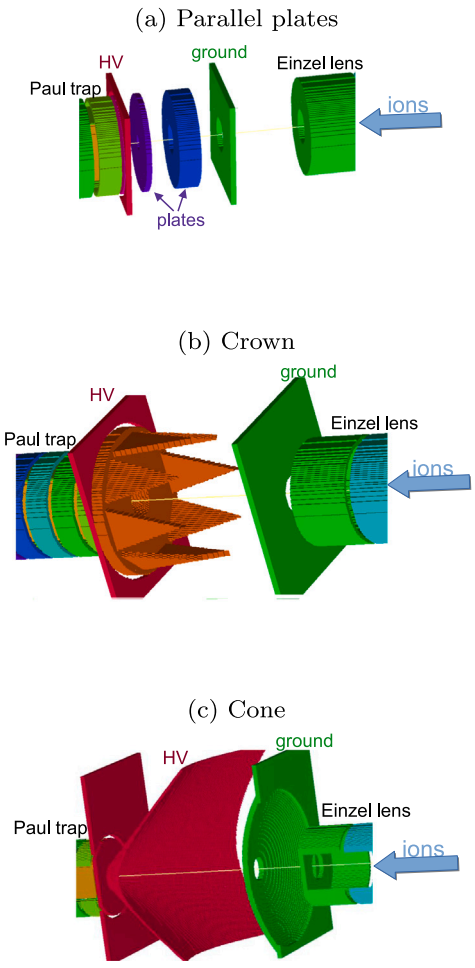

Fig. 3. Geometries studied to identify the best injection optics for MIRACLS' Paul trap. Ions enter the trap from the right side and are focused by an Einzel lens. The linear Paul trap itself is placed directly behind the endcap, which is biased to high voltage (HV). **(a)** Two additional parallel plates between ground and high voltage. **(b)** A crown-shaped electrode on HV, surrounded by a cylindrical electrode on ground (not shown in the figure). The minimum distance between crown and ground electrode was 3 cm. **(c)** A HV-cone and hyperbole on ground potential.

Third, the ion transfer between the two pressure regions is investigated (Section 4.2). Fourth, the ion extraction and re-acceleration is simulated for different extraction geometries (Section 4.3.1) as well as for different buffer-gas pressures and temperatures in pressure region 2 (Section 4.3.2). Finally, the impact of space charge on the properties of the extracted ion bunches is studied when many ions are simultaneously confined in the potential well of pressure region 2 (Section 4.3.3).

In each simulation step, 10 sets of 100 individual ions are simulated for each configuration (ion species, beam emittance, geometry, pressure, and temperature), from which the mean and the standard deviation of the observable of interest is obtained.

4.1. Injection into the high-pressure region of the Paul Trap

4.1.1. Identifying the injection geometry

The Paul trap for MIRACLS requires suitable injection optics to decelerate a 40 – 60 keV beam with a transversal emittance of $\epsilon_{\mathrm{rms}} \approx 5 - 6\,\pi$ mm mrad,[3] as expected from an ISOLDE beam [33,44]. Three

[3] If not stated otherwise, the emittance in this work is given as rms emittance.

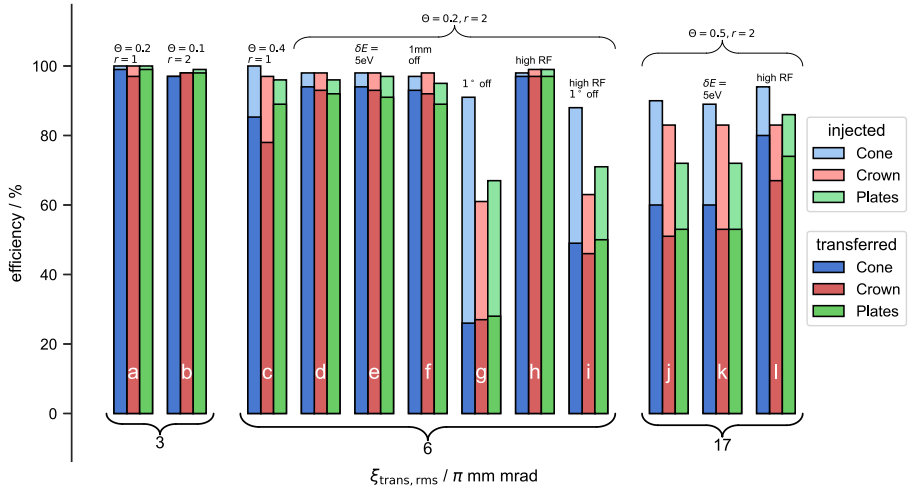

Fig. 4. Efficiency during ion beam injection for different injection geometries and various incoming beams of $^{20}Mg^{+}$ ions with transverse emittances of 3, 6 and 17 π mm mrad. Θ (in °) and r (in mm) denote the angular and the radial standard deviation of the beam, respectively. Further annotations above each beam type indicate unique properties, e.g. a 1 mm or 1° offset with respect to the Paul-trap axis, and a 5 eV energy spread (one standard deviation) of the incoming beam. The label *injected* counts the ions which entered the trap through the injection hole and *transferred* the ones which successfully traveled to the opposite axial end of the pressure region 1, i.e. next to the separation plate. The letters on the bars are used in the text for guiding the reader. The square-wave RF field has an amplitude of 120 V and a frequency of 1.2 MHz, except for *high RF* with 200 V at 2 MHz. Unless indicated otherwise, the incoming beam is simulated with an idealized monochromatic energy, i.e. its energy spread is set to zero.

different injection optics are simulated in SIMION (see Fig. 3): simple parallel plates [27], a crown surrounded by a tube (the tube is not shown in the figure) following the concept discussed in Ref. [52][4], and a cone with an angle of ∼50° with respect to the beamline axis, similarly to what is used in Ref. [40]. Other geometries, such as the one used for the BECOLA [28] and CANREB [53] buncher, likely provide better injection efficiency, but conflict with some of MIRACLS' design constraints. For instance, they require a third pressure region and would, thus, increase the length and costs of the device.

In all approaches, an Einzel lens is positioned in front of the Paul trap and its injection optics as a first ion optical element to focus the incoming beam. The injection hole at the entrance of the Paul trap had a radius of 3 mm for the first simulations and is reduced to 2.5 mm from Section 4.1.2 onwards because gas-flow simulations show more favorable differential pumping for the smaller hole size. Several ion distributions with different (transverse) emittances are investigated in the simulations. Radial and angular components of these ion ensembles are Gaussian distributed.

In all cases, the beam energy of incoming $^{20}Mg^{+}$ ions is set to 40 keV and the energy spread is zero, unless otherwise specified. The trap itself is floated to a fixed value of $U_{\text{bias}} = 39.9$ keV. Hence, the ions enter the trap with an energy of ∼100 eV. A lower entrance energy would facilitate better ion stopping in the buffer gas but would lead to increased radial losses due to the increased beam size during deceleration. We perform these first simulations without buffer gas to also investigate this radial expansion for different injection optics and how well it can be counteracted by the radially re-centering RF field. For this reason, ions are counted as "injected" when they successfully pass the entrance aperture and as "transferred" when they reach the opposite end of region one.

In order to identify the best geometry, the distances and dimensions as well as the potentials applied to the injection electrodes of each configuration of Fig. 3 and to the Einzel lens are optimized by scanning over a large parameter space. Since the acceptance of a Paul trap depends on the phase of the RF field, each ion distribution is injected at several RF phases and the minimum acceptance is taken as result, reflecting the worst case scenario.

The results of the comparison are summarized in Fig. 4. The difference between the number of injected and transferred ions can be sizable in some configurations. This is due to the strong radial dispersion of the beam during to the deceleration, especially for beams with large transverse emittance. This can be partly counteracted by a stronger RF field (h, l in Fig. 4). Beams with low emittance (≈ 3 π mm mrad) can be injected and transferred in all injection geometries with barely any ion losses (a, b in Fig. 4). Furthermore, beams with an offset in radial position of 1 mm (f) pose no serious problem for the optics, but an angular offset of 1° (g, i) leads to significant losses.

An energy spread of 5 eV barely reduces the acceptance (e, k). This is not surprising given the rather large entrance energy of around 100 eV. Another observation is that with increased emittances, the cone offers higher injection and transfer efficiencies than the other two options. Even with incoming beams with emittances as large as 17 π mm mrad and the nominal RF field strength of 120 V amplitude at 1.2 MHz, an efficiency for transferred ions of 50 to 60% is achieved (j, k, l). For this reason, the cone design is found to be the overall best option.

4.1.2. Capture efficiency

Utilizing the cone-shaped injection electrodes, this section focuses on the efficiency of the ion capture and cooling process into the axial potential minimum within the first (high-pressure) region of the Paul trap. To this end, a realistic interaction potential is used for atom-ion collisions in IonCool simulations. A 40 keV ion beam with a transverse emittance of $\xi_{\text{trans,rms}} \approx 5\,\pi$ mm mrad and an energy spread of $\Delta E = 1$ eV (one standard deviation)[5] is used for the following simulations. At the starting point, the ion ensemble is Gaussian distributed in radial position with random radial velocities, chosen to obtain a certain emittance. A linear pressure gradient of helium buffer gas from perfect vacuum at a distance of 10 mm from the injection hole to the nominal pressure inside the trap, reached at the injection hole, is applied to model the results from gas-flow simulations (see Fig. 2). In the simulation, the floating potential of the trap is optimized for each temperature and pressure to obtain maximum efficiency, ranging from $U_{\text{bias}} = 39.95$ keV to 39.99 keV.

[4] Note that the crown design was initially foreseen for up to a few kiloelectronvolt. Operation at much higher voltages might increase the risk of high voltage discharges.

[5] The energy spread of ion beams at ISOLDE may vary with the ion source utilized. Certain ion beams may thus exhibit larger energy spreads, potentially leading to reduced efficiencies compared to the values reported here.

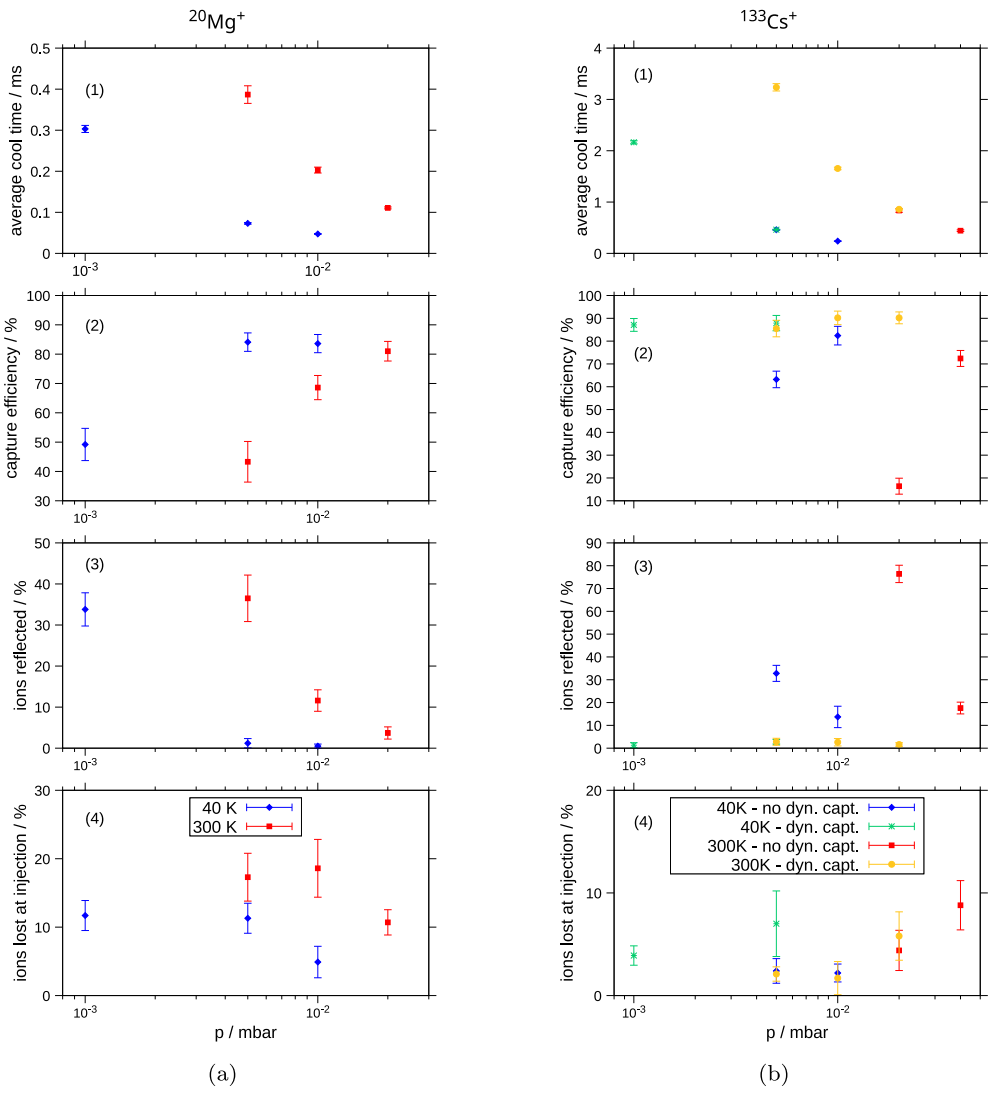

Fig. 5. Ion capture into the trapping region 1 for **(a)** $^{20}Mg^+$ and **(b)** $^{133}Cs^+$ ions. The results are obtained from IonCool simulations (using the n-4-6 potential) of the injection at 40 K and 300 K. **(1)** Average cooling time into the trap minimum. **(2)** Fraction of ions which are trapped and cooled, i.e. captured into the potential well of pressure region 1. **(3)** Ions which enter the Paul trap, but are reflected at the separation plate and leave the trap on the injection side again. **(4)** Ions which are lost at the injection region before entering the trap. 'dyn. capt.' stands for dynamic capture as explained in the text.

In the following, the capture efficiency is defined as the fraction of ions, which are successfully injected and subsequently trapped at the minimum of the axial potential well. Fig. 5(a) shows the capture efficiency and the cooling time for $^{20}Mg^+$ ions at buffer gas temperatures of 40 K and 300 K, respectively. In this context, we define the cooling time of a given ion as the time until the ion is less than 1 mm from the trap minimum in any direction and simultaneously has a momentary kinetic energy lower than 25.9 meV for 300 K and 3.4 meV for 40 K, respectively.

The average cooling time of the $^{20}Mg^+$ ions is very short (< 1 ms) for all explored pressures and temperatures, see Fig. 5(a)(1). However, the capture efficiency, as shown in Fig. 5(a)(2), drops with lower gas density. This is mainly due to ions which are reflected on the opposite axial end of the first pressure region and leave the Paul trap at the injection side, as they lose insufficient energy in the first passing, see Fig. 5(a)(3). These losses can be mitigated for injection of ion beams by using dynamic capture (dyn. capt.), i.e. switching the injection endcap to a higher potential after the ions have entered the trap. This works efficiently only for already bunched beams. At ISOLDE, the linear Paul trap ISCOOL [44] could operate in such a role of a 'pre-buncher' for MIRACLS' cryogenic trap. Additional ion losses are observed in the injection region before entering the trap, see Fig. 5(a)(4), or may occur radially inside the trap.

A second set of simulations is performed for $^{133}Cs^+$ ions as shown in Fig. 5(b). The reduced stopping power of the He gas for heavier ions can lead to significant ion losses, especially at lower gas densities. This loss mechanism persists at room temperature even for pressures as high as $2{\cdot}10^{-2}$ mbar, see Fig. 5(b)(3). However, the capture efficiency of around 15% for continuously injected beams at $2 \cdot 10^{-2}$ mbar can be increased by dynamic capture to 90%, independently of the gas density, if the incoming beam is already bunched. The cooling time is not affected by the mode of injection, see Fig. 5(b)(1).

Compared to lighter ions, a longer cooling time has to be anticipated, but with up to a few milliseconds for $^{133}Cs^+$ ions it is still shorter than the lifetime of most radionuclides available at low-energy branches at RIB facilities. While for $^{20}Mg^+$ ions an adjustment of the floating potential of the Paul trap as a function of temperature and pressure is necessary to achieve optimal efficiency, the injection of $^{133}Cs^+$ ions proves to be much less sensitive to this parameter. It is hence kept at $U_{bias} = 39.99$ keV for all $^{133}Cs^+$ simulations.

Overall, it is shown that stopping and trapping of ions is feasible for light and heavier ions with an efficiency > 80% (higher efficiency could be achieved by stronger RF fields, if technically available), while for

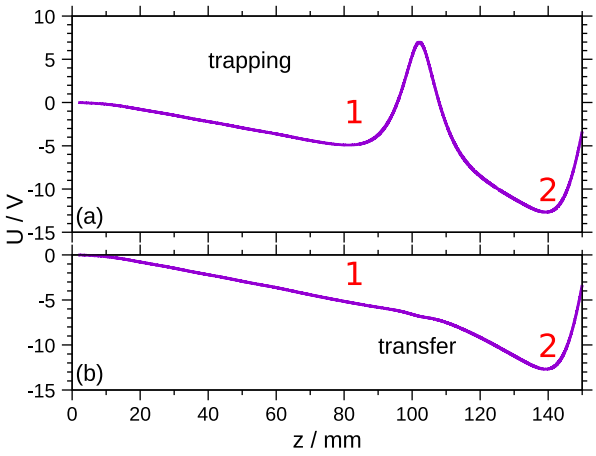

Fig. 6. Electrostatic potential along the trap axis as generated by the DC electrodes of the two pressure regions. Note that the DC component of the RF rods was set to 0 V with respect to U_{bias}. **(a)** Ions are trapped in region 1 and/or region 2. **(b)** The separator plate is switched from +10 V during trapping to −6.9 V in order to transfer the ion bunch from region 1 to region 2.

even heavier species dynamic capture, a longer trap, or – for operation at room temperature – a heavier buffer gas (e.g. argon) would be beneficial.

4.2. Ion transfer between the pressure regions

Re-heating of the cold ion cloud by collisions with helium gas in the extraction and re-acceleration regions of the trap worsens the beam quality. The straightforward way to limit the collision probability outside of the trap, is to reduce the buffer-gas pressure in the trap itself. However, this reduces stopping power and cooling efficiency for incoming ions. In order to circumvent these conflicting requirements for incoming and extracted ions, the trap is divided into a high- and low-pressure region which is expected to result in a pressure difference of about one order of magnitude, see Section 3.

The proposed axial potential of the two pressure regions created by the DC electrodes along the trap axis is shown in Fig. 6. Ions are first cooled, accumulated and bunched into the trap minimum of region 1 (Fig. 6a). Then, the voltage of the separator plate is switched down in order to pull the ion bunch into region 2 (Fig. 6b). Afterwards, the separator plate is switched up again and the next bunch can be collected. This 2-step process is required to efficiently cool the ions in the high-pressure region before they are transferred into the low-pressure region. Moreover, ions can be accumulated independently in the first trap while an ion bunch is prepared for extraction in the second trap.

The cooling time after the ion transfer tends to be longer than for the injection, since the pressure and therefore the capability to cool the ions is reduced in pressure region 2. For $^{20}Mg^{+}$ ions, the simulations show that the transfer efficiency is close to 100% for sufficiently high gas densities. Eventually, the efficiency drops with decreasing pressure due to ion losses in radial direction (e.g. to ≈75% at 40 K and 10^{-4} mbar). However, by using a stronger RF field the transfer efficiency could be increased. On the other hand, the transfer efficiency for $^{133}Cs^{+}$ ions is always 100%, but the cooling time of the ion cloud took longer than 10 ms at low pressures. Such a long cooling time of heavy ions could become a concern for MIRACLS if very short-lived isotopes are probed. In this case, a compromise between cooling time and emittance after re-acceleration has to be made.

4.3. Extraction and re-acceleration

The ion distribution obtained after re-acceleration to a few tens of kilo-electronvolts out of the Paul trap is a key aspect for MIRACLS. Hence, it is important to understand the influence of the trap's operation parameters (e.g. extraction electrodes, extraction mode, gas density) on the beam emittance. For all following simulations, the phase of the RF-field is locked during ion extraction to avoid RF distortions.

4.3.1. Geometry of the extraction optics

The first simulations of the extraction region are done by simply inverting the injection geometry (Fig. 7a) and applying the hard-sphere model for ion-gas collisions. Ions are extracted by lowering the endcap potential from +15 V to −10 V. However, these simulations reveal that the re-heating effect due to collisions of ions with He atoms in the re-acceleration path becomes critical in such a design. A strong electric field gradient outside the Paul trap quickly accelerates the ions to higher energies which makes the impact of collision with helium atoms in this region more severe in terms of ion energy loss and ion trajectory. Hence, different extraction geometries (see Fig. 7) are investigated to reduce the electric field gradient in the collision region, i.e. the fraction of the acceleration path during which the helium gas pressure has not yet dropped to zero. A common feature of the tested geometries is thus additional acceleration stages, which enable a small field gradient directly after the trap followed by the main acceleration in a second step. This choice is motivated by the results from gas-flow simulations (see Fig. 2), which yielded a similar pressure gradient for all extraction geometries (e.g. no cone, single cone or double cone as shown in Fig. 7). Since the pressure drops around one order of magnitude within 10 to 15 mm on the extraction side, re-heating will take mainly place directly after the extraction endcap. Thus, facilitated by the two-stage approach a strong electric field and thus ion acceleration is avoided in this region.

Simulations are performed using $^{20}Mg^{+}$ ions with the buffer-gas temperature set to 40 K. Ions are created close to the potential minimum of the low pressure region, where they interact with the buffer gas. A trapping time is chosen depending on the gas density such that the ions are fully thermalized prior to their extraction.

A comparison of the resulting energy spread of $^{20}Mg^{+}$ ions as a function of pressure for the four different extraction geometries is shown in Fig. 8a. A second extraction electrode, with a potential difference of only 10 V between first and second stage, greatly reduces the energy spread compared to a single cone. A more detailed analysis is given in Fig. 8b. With a single cone, a collision with a He atom during extraction can alter the ion's energy up to several tens of electronvolts while for the multistage approach it is only a few electronvolts.

Note that the cross sections calculated by the hard-sphere model might not be accurate for higher energies. In particular, the hard-sphere model assumes isotropic scattering and a cross section which is independent of an ion's kinetic energy. Both assumptions are generally not valid for higher beam energies, see for instance Ref. [55–57]. In fact, cross sections of ions scattered by neutral atoms are eventually decreasing with rising ion beam energy. Thus, we consider the present simulation results as an upper limit on how much the extracted ion bunch might be affected by collisions with He atoms within its extraction and re-acceleration path. We expect the actual experimental impact of this re-heating effect on the ion distribution to be smaller.

A comparison of the multistage geometries (Fig. 8a) reveals that the double cone (Fig. 7b) and the two stages (Fig. 7c) yield similar results. Three stages (Fig. 7d) do not provide any additional benefit compared to two stages, due to the lack of buffer gas between stage two and three in the simulations. Motivated by the consideration that the double cone might be better suited as injection geometry if re-injection from the ejection side is desired, the double cone is used for further simulations.

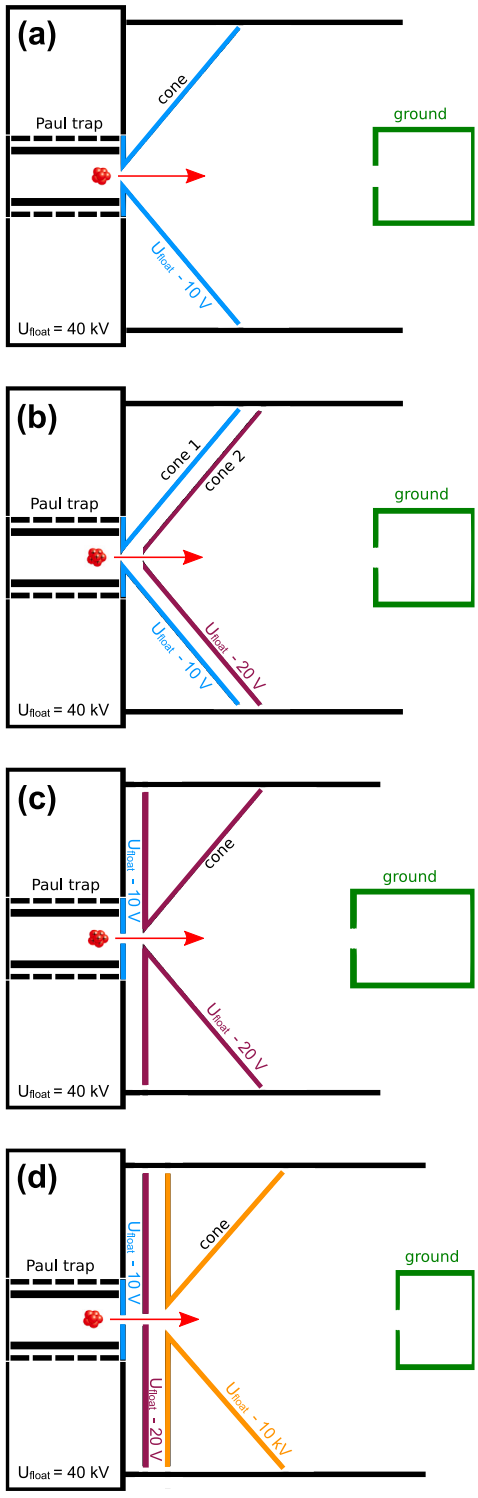

Fig. 7. Investigated geometries of the extraction optics. In (a), a single extraction cone is employed which is connected to the Paul trap's extraction endcap. Moreover, two acceleration stages are introduced, either as a double cone (b) or a simpler 2-stage design (c). The distance and voltage difference between endcap and this second acceleration stage is set to 10 mm and 10 V, respectively. **(d)** A third acceleration stage is introduced at 10 mm distance from the second stage while the voltage gradient was increased. This last investigated geometry is similar to the one discussed in Ref. [54].

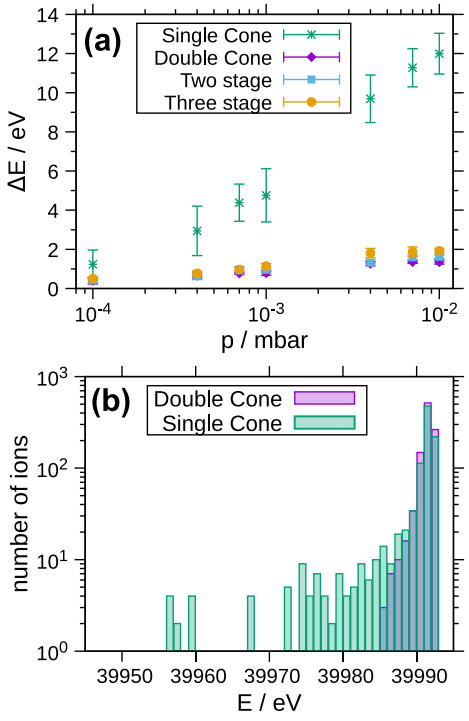

Fig. 8. **(a)** Energy spread of a $^{20}Mg^{+}$ ion ensemble (as defined by one standard deviation of the asymmetric energy distribution) after re-acceleration to 40 keV out of the Paul trap for the geometries shown in Fig. 7. To model the He-gas pressure outside the trap, a linear pressure gradient from the trap endcap to 10 mm outside the trap towards 0 mbar is assumed. **(b)** Energy distribution of 1000 ions in 1 eV steps at 10^{-3} mbar for the single and double cone geometry.

4.3.2. Room temperature vs. cryogenic temperature

The main motivation for cryogenic temperatures in the MIRACLS Paul trap is to reduce the ion beam emittance. A comparison between room temperature and cryogenic temperatures for $^{20}Mg^{+}$ and $^{133}Cs^{+}$ ion bunches using the double cone extraction geometry and employing the realistic ion-buffer gas interaction from IonCool is given in the following.

The ions are extracted from the trap by lowering the endcap potential from +2 V to −18 V, see Fig. 9. This leads to smaller energy spreads compared to the stronger field gradient typically applied for MR-ToF mass separation, for which a small temporal width of the ion bunch at the time focus point is desired. The ion cloud's properties are evaluated at a transverse plane in a field-free region inside the grounded tube, shown on the right side of Fig. 7. Note that this position is not necessarily the time focus point at which the temporal ion-bunch width Δt would be the smallest. Thus, the given Δt serves to compare this ion bunch property for different pressures and temperatures (at a fixed distance from the trap). For the estimation of longitudinal and transverse emittances all correlations between conjugate variables are taken into account (see Eqs. (A.3) and (A.4)), ensuring their accurate determination even when not evaluated at the spacial or time focus points.

A strong pressure dependence of the beam properties (temporal width of the ion bunch, energy spread, longitudinal and transverse emittance) can be seen for $^{20}Mg^{+}$ ions in Fig. 10. At higher pressures the positive effect from cryogenic temperatures is reversed due to strong re-heating caused by the larger gas density at 40 K. Below a certain pressure threshold the effect of re-heating appears to be minimized, which is around 10^{-3} mbar for 300 K and around 10^{-4} mbar for 40 K. This confirms the necessity of the second low pressure region in the trap operating at sufficiently low gas densities.

For pressures at and below 10^{-4} mbar where re-heating during re-acceleration is minimized, a fairly good agreement within a factor 1.5 is

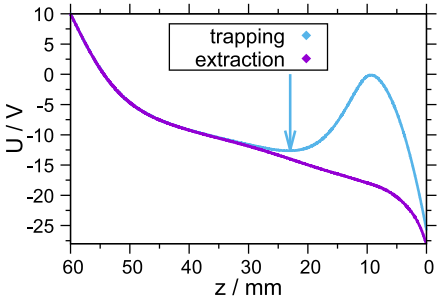

Fig. 9. Electrostatic potential along the trap axis as generated by the DC electrodes in the second pressure region. The arrow indicates the potential minimum during trapping. Note that the DC component of the RF rods was set to 0 V with respect to U_{bias}.

found between the simulated longitudinal and transverse emittance and the theoretical ones (indicated with solid lines in Fig. 10c,d), calculated with Eq. (3) and (4). Potentially, the simulations for $^{20}Mg^{+}$ are not fully converged yet and there are still effects from re-heating present. The linear dependence of the emittance on the temperature is reproduced by the simulations. According to the simulations, a reduction in emittance by a factor of 6 can be expected when lowering the buffer-gas temperature from room temperature to 40 K. This agrees rather well with the theoretical improvement by a factor 7.5.

For $^{133}Cs^{+}$ ions the longitudinal and transverse emittance are in even better agreement with the theoretical prediction, see Fig. 10d. Also here, a factor of 6 improvement at cryogenic temperatures is obtained.

In contrast to $^{20}Mg^{+}$ ions, the pressure dependence of the ion-beam emittance is less pronounced for $^{133}Cs^{+}$ ions. This is due to a reduced energy transfer during collisions with He buffer gas for heavier ions compared to lighter ones. Thus, the influence of re-heating during extraction and re-acceleration is much smaller for ^{133}Cs ions. This implies that the second region of the trap could be operated at higher pressures for heavier ion species.

At 300 K, the temporal ion-bunch width of the $^{133}Cs^{+}$ ion sample is with $\Delta t \approx 0.6\,\mu s$ larger compared to all previously studied examples. Therefore, a faster extraction mode (i.e. steeper field gradient during ejection at the position of the trap minimum) might be needed, which increases energy spread. However, the energy spread could be still sufficiently small for high-resolution laser spectroscopy, considering that it is found to be below 0.3 eV in the present extraction scheme.

Relating these results for ion extraction to the results from the ion transfer between the two pressure regions of the trap (see Section 4.2) demonstrates, that for $^{133}Cs^{+}$ the second region of the trap could be operated at 10^{-2} mbar for 300 K and 10^{-3} mbar for 40 K. At these pressure levels, the cooling time is reasonably small and re-heating during re-acceleration is reduced (see Fig. 10).

Identifying the best compromise in gas density between optimal ion transfer and lowest emittance is more demanding for $^{20}Mg^{+}$ ions. Gas densities which offer the lowest emittance lead to higher losses during the transfer from pressure region 1 to region 2 of the trap. As an already mentioned remedy to this challenge, a stronger RF field could increase the transfer efficiency.

In general, the choices of pressure and extraction mode have to be made on a case-by-case basis. Such a decision depends on several factors, like emittance and efficiency requirements, the ion mass or the half-live of the trapped radionuclides. Most importantly, these results demonstrate in simulation that a cryogenic Paul trap can provide ion beams of largely improved emittance, beneficial not just for MIRACLS but several other experiments as well (see Section 5).

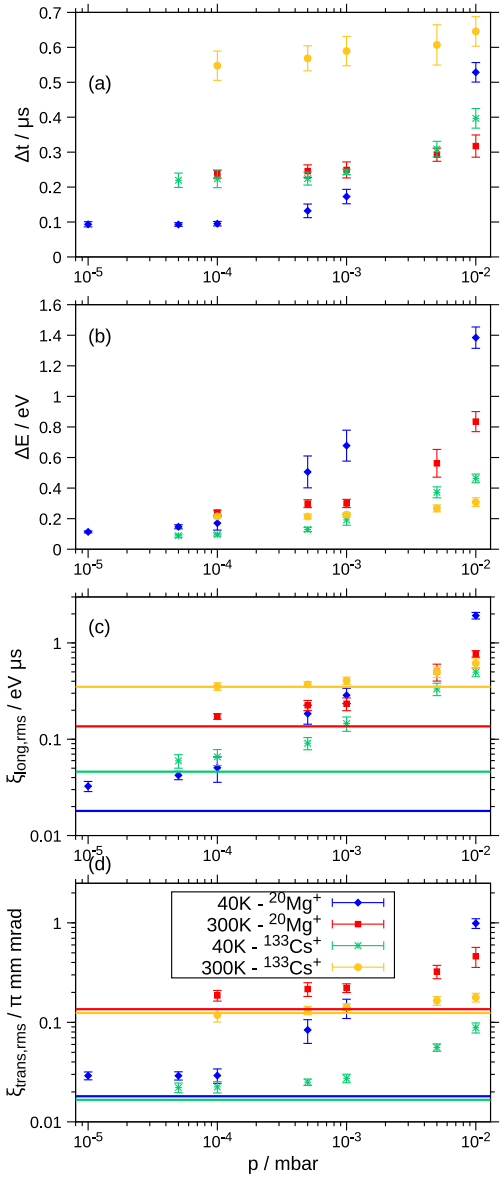

Fig. 10. Properties of ejected $^{20}Mg^{+}$ and $^{133}Cs^{+}$ ion bunches. **(a)** The temporal width of the extracted ion bunch and **(b)** its energy spread (both expressed as one standard deviation of the respective distribution) as well as **(c)** longitudinal and **(d)** transversal emittance are compared between cryogenic and room temperature buffer-gas cooling. The results are obtained using IonCool for ions after extraction from the Paul trap and re-acceleration to 40 keV. The solid lines indicate the theoretical limits calculated with Eq. (3) and (4).

4.3.3. Influence of space charge inside the ion trap on the extracted ion bunches

Space-charge effects can become a severe challenge when dealing with large ion numbers. In this case, ion-cloud properties in the trap are altered due to Coulomb repulsion between the interacting ions. As a result, the quality of the extracted ion bunch may deteriorate. In principle, MIRACLS is designed to operate with very exotic isotopes and thus, small numbers of simultaneously trapped ions are expected (initially 10^{2}-10^{4}; even less at a later stage of the project). The effect of space charge is assumed to be negligible in this case. However, using MIRACLS as mass separator [58] or in case of a large amount of (isobaric) contaminants in the ISOLDE beam, space-charge effects may play an important role and could affect the performance of the Paul trap. Therefore, space-charge simulations are carried out in SIMION using its charge-repulsion method [59].

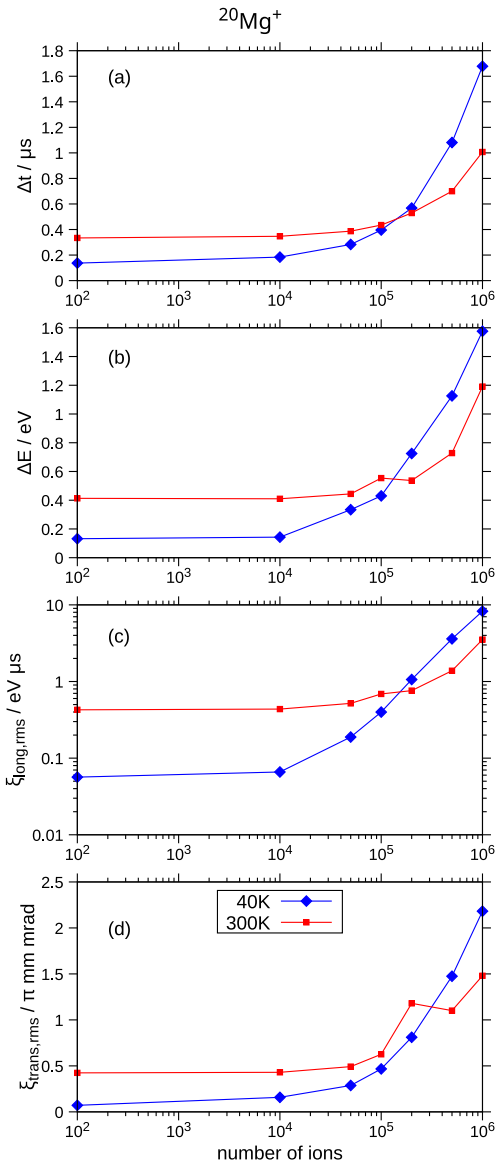

Fig. 11. Comparison of the **(a)** temporal width of the ion bunch and **(b)** its energy spread (both expressed as one standard deviation of the respective distribution) as well as **(c)** longitudinal and **(d)** transversal emittance for $^{20}Mg^+$ ion bunches extracted and accelerated to 40 keV as a function of ion number inside the Paul trap. Charge repulsion between each ion is implemented, while the effect of re-heating is neglected (i.e. the pressure is set to zero during the extraction). Each ion from an initial distribution of 100 cooled ions is attributed with a charge multiplication factor to mimic larger ion numbers, see text for details.

Already for 100 simultaneously trapped ions, the explicit application of the Coulomb repulsion between all ions is computationally expensive. In order to study larger ion ensembles without increasing the computing time, a charge multiplication factor is applied [60]. As an example, by using a charge multiplication factor of 10, each ion acts as a bunch of 10 ions. While this method may lack accuracy due to the neglect of the perturbation of the electric field by the ions' cloud charge density, it is expected to provide, in a time-efficient manner, a qualitative understanding of space-charge effects at play in the Paul trap. We have successfully applied the same method in Ref. [6,58] to study space-charge effects in the MR-ToF device of MIRACLS' low-energy apparatus.

According to the simulation results in Fig. 11, space charge does not pose a problem for up to 10,000 simultaneously stored ions at 40 K and 100,000 ions at 300 K. On the other hand, when trapping even larger ion ensembles of more than 100,000 ions in the Paul trap, the advantage of cryogenic cooling vanishes. In fact, cryogenically cooled ions are confined to a tighter space in the trap than their room temperature counter parts and thus, space-charge effects appear already at a smaller amount of ions. These results indicate the importance of operating the cryogenic Paul trap at MIRACLS only with ion numbers below 10^5 at a time.

5. Conclusions

Ion-optical simulations have been performed to characterize a cryogenic buffer-gas filled Paul trap for a next-generation application of MIRACLS' 30-keV apparatus with the goal to provide ion bunches with very low emittance. The simulations confirm theoretical considerations according to which the ion-beam emittance after re-acceleration out of the trap scales linearly with the temperature of the buffer gas. Such small emittances are beneficial for high-resolution collinear laser spectroscopy at MIRACLS, but will also be of advantage for other experiments at radioactive ion beam facilities. For example, the combination with beam-purification capabilities of the MIRACLS MR-ToF device makes a specialized cryogenic cooler-buncher also attractive for several other experimental programs at radioactive ion beam facilities, such as MR-ToF mass spectrometry and separation [58], laser spectroscopy of radioactive molecules [29] or the antiProton Unstable Matter Annihilation (PUMA) experiment [31].

CRediT authorship contribution statement

S. Lechner: Writing – review & editing, Writing – original draft, Visualization, Methodology, Investigation, Formal analysis, Data curation, Conceptualization. **S. Sels:** Writing – review & editing, Validation, Methodology, Investigation, Conceptualization. **I. Belosevic:** Writing – review & editing. **F. Buchinger:** Writing – review & editing, Funding acquisition. **P. Fischer:** Writing – review & editing, Investigation. **C. Kanitz:** Writing – review & editing, Validation, Investigation. **V. Lagaki:** Writing – review & editing, Investigation. **F.M. Maier:** Writing – review & editing, Validation, Investigation. **P. Plattner:** Writing – review & editing, Investigation. **L. Schweikhard:** Writing – review & editing, Resources, Investigation. **M. Vilen:** Writing – review & editing, Investigation. **S. Malbrunot-Ettenauer:** Writing – review & editing, Writing – original draft, Validation, Supervision, Resources, Methodology, Funding acquisition, Conceptualization.

Declaration of competing interest

The authors declare that they have no known competing financial interests or personal relationships that could have appeared to influence the work reported in this paper.

Data availability

Data will be made available on request.

Acknowledgments

The research leading to these results has received funding from the European Research Council (ERC) under the European Union's Horizon 2020 research and innovation programme under grant agreement No. 679038. The work of F.M.M. has been sponsored by the Wolfgang Gentner Programme of the German Federal Ministry of Education and Research (grant no. 05E18CHA). We are grateful for support of the MIRACLS project from CERN, the ISOLDE Collaboration, and the Max–Planck-Institut für Kernphysik (MPI K) in Heidelberg. This work is supported by the CERN Budget for Knowledge Transfer to Medical Applications and by the Natural Sciences and Engineering Council of Canada (NSERC). TRIUMF receives federal funding via a contribution agreement with the National Research Council of Canada. We would like to thank C. Fruböse for carrying out the gas-flow simulations with COMSOL®.

Table A.1
Parameters used for the (n-4-6) interaction potential in IonCool. Note that uncertainties from the fit are not included in the simulations.

	n	B/eV Å^n	C_4/eV Å^4	C_6/eV Å^6
Mg^+-He	8.0(2)	819(119)	1.474	62(6)
Cs^+-He	12	5357	1.48	12.94

Appendix. Simulation details

A.1. Convergence

The maximum time step in the simulation is chosen as a tenth of an RF period, but usual time steps internally used by the programs SIMION and IonCool are even smaller. For creating the electric field maps in SIMION, a convergence objective of 10^{-7} V is used. For the injection and extraction simulations a grid resolution of 0.5 mm/gu (grid unit) is chosen, which is reduced to 0.3 mm/gu for the simulation of the ion transfer between the two pressure regions. To justify this choice of resolution, we have compared the longitudinal and transversal emittance obtained from the double-cone extraction geometry (Fig. 7b) for 0.2 mm/gu and 0.5 mm/gu in SIMION. A higher resolution does not alter the simulation results, but would greatly increase the computational demands.

A.2. Use of IonCool

For simulations performed in IonCool [51], the electric field maps are imported from SIMION. Two models are available for ion-buffer gas interactions, the hard sphere model and the more realistic (n-4-6) potential

$$V(r) = \frac{B}{r^n} - \frac{C_4}{r^4} - \frac{C_6}{r^6} \tag{A.1}$$

with the parameters n, B, C_4 and C_6. The first term is the short-range repulsive part of the interaction, the second term describes the attraction between the ion charge with the induced electric dipole moment of the neutral atom and the third term accounts for the attraction by quadrupole polarizability. C_4 can be calculated by the expression [61]

$$C_4 = \frac{q^2\alpha}{2} \tag{A.2}$$

where q is the ion charge and α is the polarizability of the neutral particle.

C_4 for Mg^+-He is calculated according to Eq. (A.2), where α for helium is taken from Ref. [62]. The other three parameters are obtained by fitting the theoretical potential energy curves of Mg^+-He from Ref. [63] to the (n-4-6) potential. The Cs^+-He interaction parameter are given in Ref. [51] and the values are listed in Table A.1.

A.3. Emittance

The root-mean-square longitudinal and transversal emittance from SIMION and IonCool simulations are derived by following formulas:

$$\xi_{\mathrm{rms,long}} = \pi\sqrt{\langle E^2\rangle\langle t^2\rangle - \langle Et\rangle^2} \tag{A.3}$$

$$\xi_{\mathrm{rms,trans}} = \pi\sqrt{\langle x^2\rangle\langle p_x^2\rangle - \langle xp_x\rangle^2} \tag{A.4}$$

Note that π in Eq. (A.4) is already part of the unit π mm mrad. Hence, it is not added to the numerical values.

References

[1] B. Schinzler, W. Klempt, S.L. Kaufman, H. Lochmann, G. Moruzzi, R. Neugart, E.W. Otten, J. Bonn, L. Von Reisky, K.P.C. Spath, J. Steinacher, D. Weskott, Collinear laser spectroscopy of neutron-rich Cs isotopes at an on-line mass separator, Phys. Lett. B 79 (3) (1978) 209–212, http://dx.doi.org/10.1016/0370-2693(78)90224-1, URL http://www.sciencedirect.com/science/article/pii/0370269378902241.

[2] P. Campbell, I.D. Moore, M.R. Pearson, Laser spectroscopy for nuclear structure physics, Prog. Part. Nucl. Phys. 86 (2016) 127–180, http://dx.doi.org/10.1016/j.ppnp.2015.09.003, URL http://www.sciencedirect.com/science/article/pii/S0146641015000915.

[3] X.F. Yang, S.J. Wang, S.G. Wilkins, R.F.G. Ruiz, Laser spectroscopy for the study of exotic nuclei, Prog. Part. Nucl. Phys. 129 (2023) 104005, http://dx.doi.org/10.1016/j.ppnp.2022.104005, URL https://www.sciencedirect.com/science/article/pii/S0146641022000631.

[4] R. Neugart, J. Billowes, M.L. Bissell, K. Blaum, B. Cheal, K.T. Flanagan, G. Neyens, W. Nörtershäuser, D.T. Yordanov, Collinear laser spectroscopy at ISOLDE: new methods and highlights, J. Phys. G: Nucl. Part. Phys. 44 (6) (2017) 064002, http://dx.doi.org/10.1088/1361-6471/aa6642.

[5] F.M. Maier, P. Fischer, H. Heylen, V. Lagaki, S. Lechner, P. Plattner, S. Sels, F. Wienholtz, W. Nörtershäuser, L. Schweikhard, S. Malbrunot-Ettenauer, Simulations of a proof-of-principle experiment for collinear laser spectroscopy within a multi-reflection time-of-flight device, Hyperfine Interact. 240 (2019) 54, http://dx.doi.org/10.1007/s10751-019-1575-x.

[6] S. Lechner, P. Fischer, H. Heylen, V. Lagaki, F.M. Maier, P. Plattner, M. Rosenbusch, S. Sels, F. Wienholtz, R.N. Wolf, W. Nörtershäuser, L. Schweikhard, S. Malbrunot-Ettenauer, Fluorescence detection as a new diagnostics tool for electrostatic ion beam traps, Hyperfine Interact. 240 (2019) 95, http://dx.doi.org/10.1007/s10751-019-1628-1.

[7] S. Sels, P. Fischer, H. Heylen, V. Lagaki, S. Lechner, F.M. Maier, P. Plattner, M. Rosenbusch, F. Wienholtz, R.N. Wolf, W. Nörtershäuser, L. Schweikhard, S. Malbrunot-Ettenauer, First steps in the development of the multi ion reflection apparatus for collinear laser spectroscopy, Nucl. Instrum. Methods Phys. Res. B 463 (2020) 310–314, http://dx.doi.org/10.1016/j.nimb.2019.04.076.

[8] V. Lagaki, P. Fischer, H. Heylen, F. Hummer, S. Lechner, S. Sels, F.M. Maier, P. Plattner, M. Rosenbusch, F. Wienholtz, R.N. Wolf, W. Nörtershäuser, L. Schweikhard, S. Malbrunot-Ettenauer, Stray-light suppression for the MIRACLS proof-of-principle experiment, Acta Phys. Bol. B 51 (2020) 571, URL https://www.actaphys.uj.edu.pl/R/51/3/571.

[9] V. Lagaki, H. Heylen, I. Belosevic, P. Fischer, C. Kanitz, S. Lechner, F.M. Maier, W. Nörtershäuser, P. Plattner, M. Rosenbusch, S. Sels, L. Schweikhard, M. Vilen, F. Wienholtz, R.N. Wolf, S. Malbrunot-Ettenauer, An accuracy benchmark of the MIRACLS apparatus: Conventional, single-passage collinear laser spectroscopy inside a MR-ToF device, Nucl. Instrum. Methods Phys. Res. A 1014 (2021) 165663, http://dx.doi.org/10.1016/j.nima.2021.165663.

[10] F.M. Maier, M. Vilen, I. Belosevic, F. Buchinger, C. Kanitz, S. Lechner, E. Leistenschneider, W. Nörtershäuser, P. Plattner, L. Schweikhard, S. Sels, F. Wienholtz, S. Malbrunot-Ettenauer, Simulation studies of a 30-keV MR-ToF device for highly sensitive collinear laser spectroscopy, Nucl. Instrum. Methods Phys. Res. A 1048 (2023) 167927, http://dx.doi.org/10.1016/j.nima.2022.167927, URL https://www.sciencedirect.com/science/article/pii/S0168900222012190.

[11] H. Wollnik, M. Przewloka, Time-of-flight mass spectrometers with multiply reflected ion trajectories, Int. J. Mass Spectrom. Ion Process. 96 (3) (1990) 267–274, http://dx.doi.org/10.1016/0168-1176(90)85127-N, URL http://www.sciencedirect.com/science/article/pii/016811769085127N.

[12] D. Zajfman, O. Heber, L. Vejby-Christensen, I. Ben-Itzhak, M. Rappaport, R. Fishman, M. Dahan, Electrostatic bottle for long-time storage of fast ion beams, Phys. Rev. A 55 (1997) R1577–R1580, http://dx.doi.org/10.1103/PhysRevA.55.R1577, URL https://link.aps.org/doi/10.1103/PhysRevA.55.R1577.

[13] W.H. Benner, A gated electrostatic ion trap to repetitiously measure the charge and m/z of large electrospray ions, Anal. Chem. 69 (20) (1997) 4162–4168, http://dx.doi.org/10.1021/ac970163e.

[14] W.R. Plaß, T. Dickel, U. Czok, H. Geissel, M. Petrick, K. Reinheimer, C. Scheidenberger, M. I.Yavor, Isobar separation by time-of-flight mass spectrometry for low-energy radioactive ion beam facilities, Nucl. Instrum. Methods Phys. Res. B 266 (19) (2008) 4560–4564, http://dx.doi.org/10.1016/j.nimb.2008.05.079, URL http://www.sciencedirect.com/science/article/pii/S0168583X08007763.

[15] A. Piechaczek, V. Shchepunov, H.K. Carter, J.C. Batchelder, E.F. Zganjar, S.N. Liddick, H. Wollnik, Y. Hu, B.O. Griffith, Development of a high resolution isobar separator for study of exotic decays, Nucl. Instrum. Methods Phys. Res. B 266 (19) (2008) 4510–4514, http://dx.doi.org/10.1016/j.nimb.2008.05.149, URL http://www.sciencedirect.com/science/article/pii/S0168583X08007660.

[16] P. Schury, K. Okada, S. Shchepunov, T. Sonoda, A. Takamine, M. Wada, H. Wollnik, Y. Yamazaki, Multi-reflection time-of-flight mass spectrograph for short-lived radioactive ions, Eur. Phys. J. A 42 (3) (2009) 343, http://dx.doi.org/10.1140/epja/i2009-10882-6.

[17] J.D. Alexander, C.R. Calvert, R.B. King, O. Kelly, W.A. Bryan, G.R.A.J. Nemeth, W.R. Newell, C.A. Froud, I.C.E. Turcu, E. Springate, P.A. Orr, J. Pedregosa-Gutierrez, C.W. Walter, R.A. Williams, I.D. Williams, J.B. Greenwood, Short pulse laser-induced dissociation of vibrationally cold, trapped molecular ions, J. Phys. B: At. Mol. Opt. Phys. 42 (15) (2009) 154027, http://dx.doi.org/10.1088/0953-4075/42/15/154027.

[18] M. Lange, M. Froese, S. Menk, J. Varju, R. Bastert, K. Blaum, J.R.C. López-Urrutia, F. Fellenberger, M. Grieser, R. von Hahn, O. Heber, K.-U. Kühnel, F. Laux, D.A. Orlov, M.L. Rappaport, R. Repnow, C.D. Schröter, D. Schwalm, A. Shornikov, T. Sieber, Y. Toker, J. Ullrich, A. Wolf, D. Zajfman, A cryogenic electrostatic trap for long-time storage of keV ion beams, Rev. Sci. Instrum. 81 (5) (2010) 055105, http://dx.doi.org/10.1063/1.3372557.

[19] F. Wienholtz, D. Beck, K. Blaum, C. Borgmann, M. Breitenfeldt, R.B. Cakirli, S. George, F. Herfurth, J.D. Holt, M. Kowalska, S. Kreim, D. Lunney, V. Manea, J. Menéndez, D. Neidherr, M. Rosenbusch, L. Schweikhard, A. Schwenk, J. Simonis, J. Stanja, R.N. Wolf, K. Zuber, Masses of exotic calcium isotopes pin down nuclear forces, Nature 498 (2013) 346–349, URL https://doi.org/10.1038/nature12226.

[20] R.N. Wolf, F. Wienholtz, D. Atanasov, D. Beck, K. Blaum, C. Borgmann, F. Herfurth, M. Kowalska, S. Kreim, Y.A. Litvinov, D. Lunney, V. Manea, D. Neidherr, M. Rosenbusch, L. Schweikhard, J. Stanja, K. Zuber, ISOLTRAP's multi-reflection time-of-flight mass separator/spectrometer, Int. J. Mass Spectrom. 349–350 (2013) 123–133, http://dx.doi.org/10.1016/j.ijms.2013.03.020, URL http://www.sciencedirect.com/science/article/pii/S1387380613001115.

[21] T. Dickel, W.R. Plaß, A. Becker, U. Czok, H. Geissel, E. Haettner, C. Jesch, W. Kinsel, M. Petrick, C. Scheidenberger, A. Simon, M.I. Yavor, A high-performance multiple-reflection time-of-flight mass spectrometer and isobar separator for the research with exotic nuclei, Nucl. Instrum. Methods Phys. Res. A 777 (2015) 172–188, http://dx.doi.org/10.1016/j.nima.2014.12.094, URL https://www.sciencedirect.com/science/article/pii/S0168900214015629.

[22] M.P. Reiter, S.A.S. Andrés, J. Bergmann, T. Dickel, J. Dilling, A. Jacobs, A.A. Kwiatkowski, W.R. Plaß, C. Scheidenberger, D. Short, C. Will, C. Babcock, E. Dunling, A. Finlay, C. Hornung, C. Jesch, R. Klawitter, B. Kootte, D. Lascar, E. Leistenschneider, T. Murböck, S.F. Paul, M. Yavor, Commissioning and performance of TITAN's multiple-reflection time-of-flight mass-spectrometer and isobar separator, Nucl. Instrum. Methods Phys. Res. A 1018 (2021) 165823, http://dx.doi.org/10.1016/j.nima.2021.165823, URL https://www.sciencedirect.com/science/article/pii/S0168900221008081.

[23] P. Chauveau, P. Delahaye, G. De France, S. El Abir, J. Lory, Y. Merrer, M. Rosenbusch, L. Schweikhard, R.N. Wolf, PILGRIM, a multi-reflection time-of-flight mass spectrometer for Spiral2-S3 at GANIL, Nucl. Instrum. Methods Phys. Res. B 376 (2016) 211–215, http://dx.doi.org/10.1016/j.nimb.2016.01.025, URL https://www.sciencedirect.com/science/article/pii/S0168583X16000732. Proceedings of the XVIIth International Conference on Electromagnetic Isotope Separators and Related Topics (EMIS2015), Grand Rapids, MI, U.S.A., 11-15 May 2015.

[24] B. Liu, M. Brodeur, D.P. Burdette, J.M. Kelly, T. Kim, J. Long, P.D. O'Malley, The performance of the commissioned notre dame multi-reflection time-of-flight mass spectrometer, Nucl. Instrum. Methods Phys. Res. A 985 (2021) 164679, http://dx.doi.org/10.1016/j.nima.2020.164679, URL https://www.sciencedirect.com/science/article/pii/S0168900220310767.

[25] M. Rosenbusch, M. Wada, S. Chen, A. Takamine, S. Iimura, D. Hou, W. Xian, S. Yan, P. Schury, Y. Hirayama, Y. Ito, H. Ishiyama, S. Kimura, T. Kojima, J. Lee, J. Liu, S. Michimasa, H. Miyatake, J.Y. Moon, M. Mukai, S. Naimi, S. Nishimura, T. Niwase, T. Sonoda, Y.X. Watanabe, H. Wollnik, The new MRTOF mass spectrograph following the ZeroDegree spectrometer at RIKEN's RIBF facility, Nucl. Instrum. Methods Phys. Res. A 1047 (2023) 167824, http://dx.doi.org/10.1016/j.nima.2022.167824, URL https://www.sciencedirect.com/science/article/pii/S0168900222011160.

[26] R.B. Moore, A.M.G. Dezfuli, P. Varfalvy, H. Zhao, The ISOLDE Collaboration, Production, transfer and injection of charged particles in traps and storage rings, Phys. Scr. T59 (1995) 93–105, http://dx.doi.org/10.1088/0031-8949/1995/t59/012.

[27] S. Schwarz, G. Bollen, R. Ringle, J. Savory, P. Schury, The LEBIT ion cooler and buncher, Nucl. Instrum. Methods Phys. Res. A 816 (2016) 131–141, http://dx.doi.org/10.1016/j.nima.2016.01.078, URL http://www.sciencedirect.com/science/article/pii/S0168900216001194.

[28] B.R. Barquest, G. Bollen, P.F. Mantica, K. Minamisono, R. Ringle, S. Schwarz, C.S. Sumithrarachchi, RFQ beam cooler and buncher for collinear laser spectroscopy of rare isotopes, Nucl. Instrum. Methods Phys. Res. A 866 (2017) 18–28, http://dx.doi.org/10.1016/j.nima.2017.05.036, URL http://www.sciencedirect.com/science/article/pii/S0168900217305892.

[29] R.F. Garcia Ruiz, R. Berger, J. Billowes, C.L. Binnersley, M.L. Bissell, A.A. Breier, A.J. Brinson, K. Chrysalidis, T.E. Cocolios, B.S. Cooper, K.T. Flanagan, T.F. Giesen, R.P. de Groote, S. Franchoo, F.P. Gustafsson, T.A. Isaev, Á. Koszorús, G. Neyens, H.A. Perrett, C.M. Ricketts, S. Rothe, L. Schweikhard, A.R. Vernon, K.D.A. Wendt, F. Wienholtz, S.G. Wilkins, X.F. Yang, Spectroscopy of short-lived radioactive molecules, Nature 581 (2020) 396–400, http://dx.doi.org/10.1038/s41586-020-2299-4.

[30] G. Arrowsmith-Kron, et al., Opportunities for fundamental physics research with radioactive molecules, 2023, arXiv:2302.02165. URL https://arxiv.org/abs/2302.02165.

[31] T. Aumann, W. Bartmann, A. Bouvard, O. Boine-Frankenheim, A. Broche, F. Butin, D. Calvet, J. Carbonell, P. Chiggiato, H. De Gersem, R. De Oliveira, T. Dobers, F. Ehm, J. Ferreira Somoza, J. Fischer, M. Fraser, E. Friedrich, J.-L. Grenard, G. Hupin, K. Johnston, Y. Kubota, M. Gomez-Ramos, P. Indelicato, R. Lazauskas, S. Malbrunot-Ettenauer, N. Marsic, W. Müller, S. Naimi, N. Nakatsuka, R. Necca, G. Neyens, A. Obertelli, Y. Ono, S. Pasinelli, N. Paul, E.C. Pollacco, D. Rossi, H. Scheit, R. Seki, A. Schmidt, L. Schweikhard, S. Sels, E. Siesling, T. Uesaka, M. Wada, F. Wienholtz, S. Wycech, S. Zacarias, PUMA: Antiprotons and Radioactive Nuclei, Tech. Rep. CERN-SPSC-2019-033. SPSC-P-361, CERN, Geneva, 2019, URL https://cds.cern.ch/record/2691045.

[32] T. Kim, Buffer Gas Cooling of Ions in a Radio Frequency Quadrupole Ion Guide : A Study of the Cooling Process and Cooled Beam Properties (Ph.D. thesis), McGill University, 1997.

[33] A. Jokinen, M. Lindroos, E. Molin, M. Petersson, RFQ-cooler for low-energy radioactive ions at ISOLDE, Nucl. Instrum. Methods Phys. Res. B 204 (2003) 86–89, http://dx.doi.org/10.1016/S0168-583X(02)01894-3, URL https://www.sciencedirect.com/science/article/pii/S0168583X02018943.

[34] D. Lunney, C. Bachelet, C. Guénaut, S. Henry, M. Sewtz, COLETTE: A linear paul-trap beam cooler for the on-line mass spectrometer MISTRAL, Nucl. Instrum. Methods Phys. Res. A 598 (2) (2009) 379–387, http://dx.doi.org/10.1016/j.nima.2008.09.050, URL https://www.sciencedirect.com/science/article/pii/S0168900208014459.

[35] F.G. Major, H.G. Dehmelt, Exchange-collision technique for the rf spectroscopy of stored ions, Phys. Rev. 170 (1968) 91–107, http://dx.doi.org/10.1103/PhysRev.170.91, URL https://link.aps.org/doi/10.1103/PhysRev.170.91.

[36] K. Blaum, F. Herfurth, Trapped Charged Particles and Fundamental Interactions, Vol. 749, Springer-Verlag Berlin Heidelberg, 2008, p. 192, http://dx.doi.org/10.1007/978-3-540-77817-2.

[37] J.A. Richards, R.M. Huey, J. Hiller, A new operating mode for the quadrupole mass filter, Int. J. Mass Spectrom. Ion Phys. 12 (4) (1973) 317–339, http://dx.doi.org/10.1016/0020-7381(73)80102-0, URL https://www.sciencedirect.com/science/article/pii/0020738173801020.

[38] L. Ding, M. Sudakov, S. Kumashiro, A simulation study of the digital ion trap mass spectrometer, Int. J. Mass Spectrom. 221 (2) (2002) 117–138, http://dx.doi.org/10.1016/S1387-3806(02)00921-1, URL https://www.sciencedirect.com/science/article/pii/S1387380602009211.

[39] L. Ding, M. Sudakov, F.L. Brancia, R. Giles, S. Kumashiro, A digital ion trap mass spectrometer coupled with atmospheric pressure ion sources, J. Mass Spectrom. 39 (5) (2004) 471–484, http://dx.doi.org/10.1002/jms.637, URL https://analyticalsciencejournals.onlinelibrary.wiley.com/doi/abs/10.1002/jms.637.

[40] T. Brunner, M.J. Smith, M. Brodeur, S. Ettenauer, A.T. Gallant, V.V. Simon, A. Chaudhuri, A. Lapierre, E. Mané, R. Ringle, M.C. Simon, J.A. Vaz, P. Delheij, M. Good, M.R. Pearson, J. Dilling, TITAN's digital RFQ ion beam cooler and buncher, operation and performance, Nucl. Instrum. Methods Phys. Res. A 676 (2012) 32–43, http://dx.doi.org/10.1016/j.nima.2012.02.004, URL http://www.sciencedirect.com/science/article/pii/S0168900212001398.

[41] M.J. Smith, A Square-Wave-Driven Radiofrequency Quadrupole Cooler and Buncher for TITAN (MSc thesis), University of British Columbia, 2005.

[42] A. Kellerbauer, T. Kim, R.B. Moore, P. Varfalvy, Buffer gas cooling of ion beams, Nucl. Instrum. Methods Phys. Res. A 469 (2) (2001) 276–285, http://dx.doi.org/10.1016/S0168-9002(01)00286-8, URL https://www.sciencedirect.com/science/article/pii/S0168900201002868.

[43] F. Herfurth, J. Dilling, A. Kellerbauer, G. Bollen, S. Henry, H.-J. Kluge, E. Lamour, D. Lunney, R.B. Moore, C. Scheidenberger, S. Schwarz, G. Sikler, J. Szerypo, A linear radiofrequency ion trap for accumulation, bunching, and emittance improvement of radioactive ion beams, Nucl. Instrum. Methods Phys. Res. A 469 (2) (2001) 254–275, http://dx.doi.org/10.1016/S0168-9002(01)00168-1, URL http://www.sciencedirect.com/science/article/pii/S0168900201001681.

[44] H. Frånberg, P. Delahaye, J. Billowes, K. Blaum, R. Catherall, F. Duval, O. Gianfrancesco, T. Giles, A. Jokinen, M. Lindroos, D. Lunney, E. Mane, I. Podadera, Off-line commissioning of the ISOLDE cooler, Nucl. Instrum. Methods Phys. Res. B 266 (19) (2008) 4502–4504, http://dx.doi.org/10.1016/j.nimb.2008.05.097, URL http://www.sciencedirect.com/science/article/pii/S0168583X08007647.

[45] S. Sels, F.M. Maier, M. Au, P. Fischer, C. Kanitz, V. Lagaki, S. Lechner, E. Leistenschneider, D. Leimbach, E.M. Lykiardopoulou, A.A. Kwiatkowski, T. Manovitz, Y.N. Vila Gracia, G. Neyens, P. Plattner, S. Rothe, L. Schweikhard, M. Vilen, R.N. Wolf, S. Malbrunot-Ettenauer, Doppler and sympathetic cooling for the investigation of short-lived radioactive ions, Phys. Rev. Res. 4 (2022) 033229, http://dx.doi.org/10.1103/PhysRevResearch.4.033229, URL https://link.aps.org/doi/10.1103/PhysRevResearch.4.033229.

[46] M. Ady, Molflow 2.6 algorithm, 2016, URL https://molflow.web.cern.ch/sites/molflow.web.cern.ch/files/molflow_docu.pdf.

[47] J.H. Moore, C.C. Davis, M.A. Coplan, S.C. Greer, Building Scientific Apparatus, fourth ed., Cambridge University Press, 2009, http://dx.doi.org/10.1017/CBO9780511609794.

[48] COMSOL multiphysics® v. 5.3, 2018, URL http://www.comsol.com/.

[49] D.A. Dahl, SIMION for the personal computer in reflection, Int. J. Mass Spectrom. 200 (1) (2000) 3–25, http://dx.doi.org/10.1016/S1387-3806(00)00305-5, URL http://www.sciencedirect.com/science/article/pii/S1387380600003055.

[50] Collision model HS1, 2021, URL https://simion.com/info/collision_model_hs1.html.

[51] S. Schwarz, IonCool - a versatile code to characterize gas-filled ion bunchers and coolers (not only) for nuclear physics applications, Nucl. Instrum. Methods Phys. Res. A 566 (2) (2006) 233–243, http://dx.doi.org/10.1016/j.nima.2006.07.004, URL http://www.sciencedirect.com/science/article/pii/S016890020601254X.

[52] W. Gins, R.D. Harding, M. Baranowski, M.L. Bissell, R.F. Garcia Ruiz, M. Kowalska, G. Neyens, S. Pallada, N. Severijns, P. Velten, F. Wienholtz, Z.Y. Xu, X.F. Yang, D. Zakoucky, A new beamline for laser spin-polarization at ISOLDE, Nucl. Instrum. Methods Phys. Res. A 925 (2019) 24–32, http://dx.doi.org/10.1016/j.nima.2019.01.082, URL https://www.sciencedirect.com/science/article/pii/S0168900219301536.

[53] B.R. Barquest, J.C. Bale, J. Dilling, G. Gwinner, R. Kanungo, R. Krücken, M.R. Pearson, Development of a new RFQ beam cooler and buncher for the CANREB project at TRIUMF, Nucl. Instrum. Methods Phys. Res. B 376 (2016) 207–210, http://dx.doi.org/10.1016/j.nimb.2016.02.035, URL https://www.sciencedirect.com/science/article/pii/S0168583X16001658.

[54] I. Podadera Aliseda, T. Fritioff, T. Giles, A. Jokinen, M. Lindroos, F. Wenander, Design of a second generation RFQ Ion Cooler and Buncher (RFQCB) for ISOLDE, Nuclear Phys. A 746 (2004) 647–650, http://dx.doi.org/10.1016/j.nuclphysa.2004.09.043, URL https://www.sciencedirect.com/science/article/pii/S0375947404009868. Proceedings of the Sixth International Conference on Radioactive Nuclear Beams (RNB6).

[55] D.W. Sida, The scattering of positive ions by neutral atoms, Philos. Mag.: A J. Theoret. Exp. Appl. Phys. 2 (18) (1957) 761–771, http://dx.doi.org/10.1080/14786435708241025.

[56] F.J. Zehr, H.W. Berry, Elastic scattering of lithium ions in helium and hydrogen, Phys. Rev. 159 (1967) 13–20, http://dx.doi.org/10.1103/PhysRev.159.13, URL https://link.aps.org/doi/10.1103/PhysRev.159.13.

[57] K.-i. Niurao, H. Inouye, Differential scattering of K+ ions (150-700 eV) in collision with Ne atoms, J. Phys. Soc. Japan 40 (3) (1976) 813–820, http://dx.doi.org/10.1143/JPSJ.40.813.

[58] F.M. Maier, F. Buchinger, L. Croquette, P. Fischer, H. Heylen, F. Hummer, C. Kanitz, A.A. Kwiatkowski, V. Lagaki, S. Lechner, E. Leistenschneider, G. Neyens, P. Plattner, A. Roitman, M. Rosenbusch, L. Schweikhard, S. Sels, M. Vilen, F. Wienholtz, S. Malbrunot-Ettenauer, Increased beam energy as a pathway towards a highly selective and high-flux MR-ToF mass separator, Nucl. Instrum. Methods Phys. Res. A 1056 (2023) 168545, http://dx.doi.org/10.1016/j.nima.2023.168545, URL https://www.sciencedirect.com/science/article/pii/S0168900223005351.

[59] A.D. Appelhans, D.A. Dahl, SIMION ion optics simulations at atmospheric pressure, Int. J. Mass Spectrom. 244 (1) (2005) 1–14, http://dx.doi.org/10.1016/j.ijms.2005.03.010, URL http://www.sciencedirect.com/science/article/pii/S1387380605001089.

[60] D. Manura, D. Dahl, SIMION 8.1 user manual, 2013, URL http://simion.com/.

[61] L.A. Viehland, E.A. Mason, W.F. Morrison, M.R. Flannery, Tables of transport collision integrals for (n, 6, 4) ion-neutral potentials, At. Data Nucl. Data Tables 16 (6) (1975) 495–514, http://dx.doi.org/10.1016/0092-640X(75)90022-4, URL http://www.sciencedirect.com/science/article/pii/0092640X75900224.

[62] M. Masili, A.F. Starace, Static and dynamic dipole polarizability of the helium atom using wave functions involving logarithmic terms, Phys. Rev. A 68 (2003) 012508, http://dx.doi.org/10.1103/PhysRevA.68.012508, URL https://link.aps.org/doi/10.1103/PhysRevA.68.012508.

[63] A.M. Gardner, C.D. Withers, J.B. Graneek, T.G. Wright, L.A. Viehland, W.H. Breckenridge, Theoretical Study of M^+-RG and M^{2+}-RG Complexes and Transport of M^+ through RG (M=Be and Mg, RG=He-Rn), J. Phys. Chem. A 114 (28) (2010) 7631–7641, http://dx.doi.org/10.1021/jp103836t, PMID: 20578713.